JTTEE5 22:772–782
DOI: 10.1007/s11666-013-9890-2
1059-9630/$19.00 © ASM International

Cold-Sprayed Ni-Al_2O_3 Coatings for Applications in Power Generation Industry

F. Sevillano, P. Poza, C. J. Múnez, S. Vezzù, S. Rech, and A. Trentin

(Submitted September 27, 2012; in revised form December 3, 2012)

Cermets coatings are extensively used in energy applications both because of their high wear resistance as required, for example, in components like gas turbine sealants, and because of their specific functionality as required in solar absorbers. So far, high-temperature thermal spraying and physical vapor deposition have traditionally been used to deposit this kind of coatings. In this study, Ni-Al_2O_3 coatings have been deposited using a Kinetic®3000 cold-spray system starting from Ni and Al_2O_3 powders blend; five blends have been prepared setting the alumina content in the feedstock to 10, 25, 50, 75, and 90 wt.%. The embedded alumina ranges between a few percent weight up to 16 and 31 wt.%, while the microhardness shows a deep increase from 175 Vickers in the case of pure Ni coatings up to 338 Vickers. The spray and coating growth mechanism have been discussed, with special attention to the fragmentation of the ceramic particles during the impact. Finally, the coating behavior at high temperature was analyzed by oxidation tests performed in air at 520 °C emphasizing a good oxidation resistance that could represent a very promising basis for application in power generation systems.

Keywords cermet coatings, cold spray, isothermal oxidation, scanning electron microscopy (SEM)

1. Introduction

Cermets coatings are formed by ceramic particles embedded in a metallic matrix. They are extensively used in several industrial applications to combine the structural integrity of metals with the higher operating temperature and wear resistance of the ceramics. These coatings exhibit better toughness and thermal sock resistance than the pure ceramic coatings, although the maximum operating temperature and thermal stability is reduced. The powder metallurgy is one of the most considered ways to obtain cermet materials thanks to the great versatility of processable materials and conditions. In this field, thermal-spray techniques are traditionally devoted to produce thin and thick protective cermet coatings and, for example, several industrial case studies in mechanic and mechatronic show that WC-Co and WC-Ni wear-resistant coatings produced mainly by high-velocity oxy-fuel (HVOF) represents today one of the most diffused and successful example of potentiality of cermet materials (Ref 1). Different powder feedstock materials could be employed to deposit cermet coatings; first of all, the use of powder blend is reported (Ref 2) and represents the easiest and more versatile approach. However, specific cermet powder feedstock such as mechanically alloyed powder (Ref 3) or core-shell coated powders (Ref 4) or simply agglomerated sintered powders are often employed to increase coating homogeneity and ceramic content in the coating.

Cermets coatings are used in energy applications mainly thanks to their high wear and oxidation resistance and their customized functionality. Wear-resistant sealants are used, for example, in gas turbines for power generation and propulsion (Ref 5-7). The gas turbine efficiency is increased by reducing the clearances between rotating and stationary components in the gas path, and the contact of abradable and abrasive coatings plays a key role in the control of the clearance. In addition, gas turbine sealants operate at extreme conditions, which include high-temperature and aggressive environment. At these conditions, cermets coatings containing Al_2O_3 or Al_2O_3-TiO_2 exhibit better performance and durability than the pure ceramic coatings also because the residual stresses developed at the interface are lower with respect to pure ceramic coatings (Ref 5-7). A further application of cermets is on solar-selective absorber materials: the interest for renewable energies has increased over the last decades. driven by rising fuel prices and more stringent regulations for reduction of emissions (Ref 8). Solar thermal power generation constitutes to be one of the most important *green energies* and is increasing the power capacity installed throughout the world. Concentrating solar power systems use solar absorbers to convert sunlight to thermal electric power. Different technologies could be used, and the most extended are parabolic troughs cylinders, where a parabolic mirror concentrates sunlight onto a cylindrical receiver, or central receiver (or power tower), where a field of heliostats focuses sunlight onto a receiver located

F. Sevillano, P. Poza, and **C.J. Múnez**, Departamento de Tecnología Mecánica, Universidad Rey Juan Carlos, Escuela Superior de Ciencias Experimentales y Tecnología, C/ Tulipán s.n., 28933 Móstoles, Madrid, Spain; and **S. Vezzù**, **S. Rech**, and **A. Trentin**, Veneto Nanotech scpa, Nanofab Laboratory, via delle industrie, 5, 30157 Marghera, VE, Italy. Contact e-mail: simone.vezzu@venetonanotech.it.

at the top of a tower (Ref 9). The efficiency of the system depends on the capability to absorb sunlight, and so the surface of the collector should be modified to get good solar properties in terms of high solar absorbance (α) and low thermal emittance (ε). From the structural point of view, the coatings should be able to operate at high temperature and surrounded by an oxidized environment (Ref 9-11). Different possibilities have been analyzed to obtain a selective surface, and most of them combine ceramic phases, to provided high α, with metallic binders which provide low ε (Ref 12). For these reasons, cermets coatings, usually formed by ceramic oxides like Al_2O_3, Cr_2O_3, or SiO_2 bound together with Ni or Mo, have been deposited onto the receiver (Ref 10-16). The system constituted of Ni matrix and Al_2O_3 filler has been selected also in this study to combine good solar performances with oxidation resistance. Among the metals, Ni has been selected as cermet matrix thanks to the excellent characteristics of cold spray (CS) coatings (Ref 17).

Cermets coatings are also used as the support of solid oxy-fuel cells, which have the potential to operate at higher electrical efficiency and with lower emissions in respect of traditional power generation techniques. These devices are electrochemical in nature, meaning that they convert fuel directly into electricity (Ref 18-20). They required high-wear resistance (Ref 5-7, 21-23) and have been usually processed by thermal-spray techniques, like plasma spraying or HVOF. However, the high temperatures involved in these processes could deteriorate the substrate properties and promote partial oxidation of the metallic powders, if a protective environment is not used. In addition, cermets coatings for solar absorbers have been traditionally deposited by physical vapor deposition. However, this process route is not feasible for power tower plants, and generally selective paints are used in these systems, although their performance is problematic from the structural and functional points of view (Ref 10, 12-16).

Cold gas dynamic spray, or simply CS, is receiving more and more attention in the recent years because of the low spraying temperature and exclusive opportunities in the deposition of metal-based materials, in particular oxygen-sensitive materials such as aluminum, titanium, and magnesium alloys. (Ref 17) CS belongs to thermal-spray techniques, however, rather than traditional flame, arc, or plasma spray; it is strictly a solid-state powder deposition process because no melting or partial melting of spraying particle is involved. In CS deposition, a carrier gas (air, nitrogen, helium, or their mixtures) is split in a first larger part of carrier flow that is heated up to 1000 °C, and a second smaller part of carrier gas that is kept cold; it carries through the powder feeder and it drags a controlled powder flow to the nozzle. Here, the two carrier gas flows are combined and accelerated passing through a de Laval nozzle. Particle velocities are reported up to 1000 m/s, while fluidodynamic models predict that powder temperature range from room temperature up to a few hundreds of degrees depending on selected gas temperature. CS does not require a protective environment to produce coatings with reduced oxides content, and has low residual stresses (Ref 24), and high efficiency. This spraying technology is a high rate material deposition process in which micrometric, unmelted, powder particles are shot to the substrate at supersonic velocities. Owing to the high velocity impact, they plastically deform and bond together building up the coating (Ref 25-27). CS has been traditionally focused on metallic coatings; however, increasing efforts are being made to deposit other materials like cermet coatings (Ref 28-30). In this field, it is reported that the addition of a low amount of ceramic particle in a pure metal feedstock leads to a slight increase in the deposition efficiency (Ref 31), but on the other side, the deposition efficiency is highly reduced for deposition of cermets with a high amount of ceramic and finally, when cold spray is performed with pure ceramic materials, even if shear instabilities are observed and reported the deposition efficiency is very low and strictly depend on the substrate materials and on the capability to induce plastic deformation on the substrate top layer as extensively reported by Kielmann et al. (Ref 30) in the case of titanium dioxide coatings. This scenario highlights the challenge to extend CS technology for depositing cermets with a high ceramic content, and in this sense, many research efforts are focused on achieving this objective. The aim of this article is to evaluate the viability to process Ni-Al_2O_3 coatings by CS deposition for power generation application. The effect of ceramic content on the coating's microstructure and high-temperature performance will be analyzed.

2. Experimental Methods

2.1 Feedstock Powders

The use of powder blends has been selected in this preliminary study to maximize the flexibility and versatility of powder feedstock preparation in terms of materials and percentages. The plan of experiment consider the effect of a wide range of ceramic/metal ratio, as reported in this article, as well as the use of different ceramic fillers and metal matrices, actually in progress, to have a complete panorama about the more promising materials from both the points of view of solar performances and wear and oxidation resistances. In a second part of the study, once the cermet average composition will be identified, customized feedstock will be expressly prepared by powder agglomeration or powder coating to further optimize the material characteristics. Ni and Al_2O_3 (both provided by H.C. Starck Amperit®; Germany) powders, with particle size of $-30+10$ and $-27+17$ μm, respectively, have been employed in this study. The micrographies of feedstock powders are shown in Fig. 1; the morphology is regular, with sharpened faces for alumina, while Ni particles exhibit spherical shapes. Five mixtures with five different alumina amount were prepared and sprayed, scanning the ceramic content in a wide range: 10-25-50-75-90 wt.%. The powders were mechanically blended for each mixture using a Turbula mixer for 70 min to prepare the feedstock for spray deposition. Two mixtures between

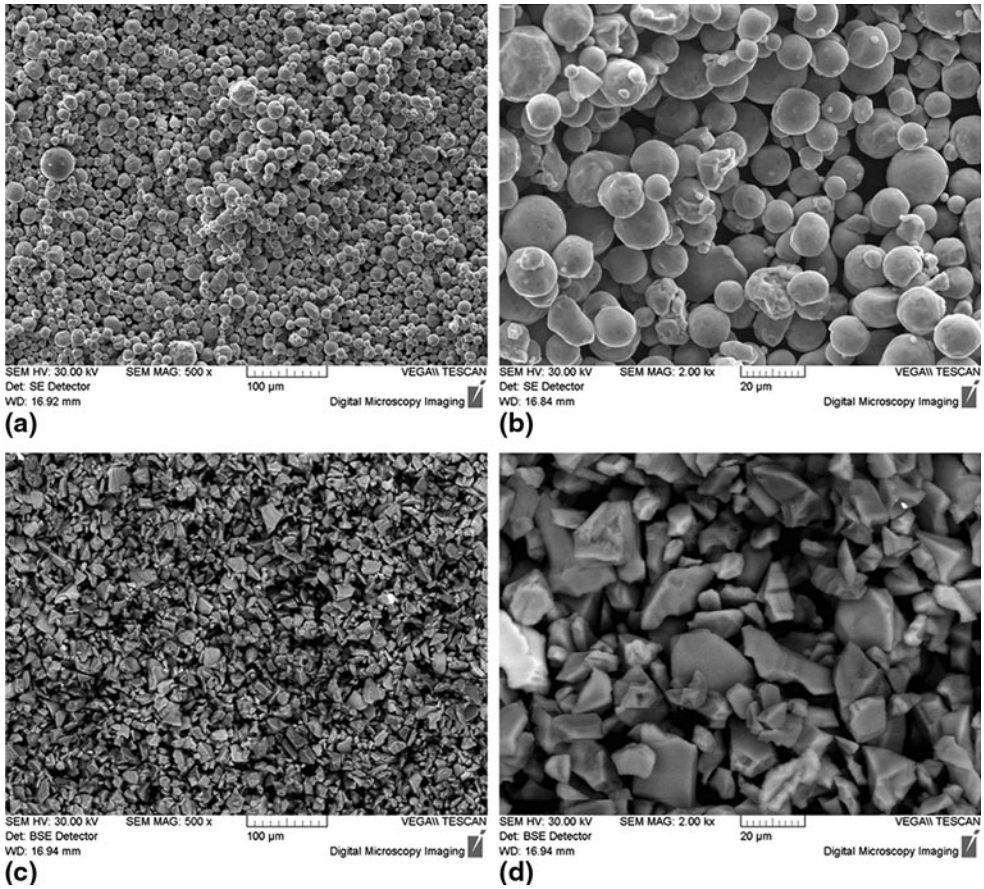

Fig. 1 Feedstock powders, SEM viewing of (a) and (b) Ni; and (c) and (d) Al_2O_3 particles

Ni powders and 5 and 10 wt.% of spherical agglomerated aluminum oxide particles, Metco 6100, has been prepared by the same procedure and tested to increase the dispersion of finer ceramic particles in the metal matrix.

2.2 Substrates

Ni-Al_2O_3 cermets coatings were deposited on grade 22 steel substrates typically employed in the fabrication of pipes and boilers for high-pressure and temperatures applications. The samples' size was $30 \times 50 \times 5$ mm^3; the surface prepared by grit-blasting with corundum of size 20 mesh and then cleaned in acetone bath for 10 min.

2.3 CS Deposition

The deposition was carried out by means of a Cold-Spray CGT-Kinetiks® 3000 (CGT Cold Gas Technology, Sultzer Metco AG, Switzerland) equipped with a metallic *Type 24* nozzle. A stainless steel 10-cm-long pre-chamber was also used to further enhance the particle temperature through contact with the hot gas; however, no quantitative results are available to quantify the particle temperature increase. The optimization and design of this pre-heated chamber has been made by Veneto Nanotech. The parameters for the cold-spray process are shown in Table 1 while Fig. 2 shows a schema of CS deposition. Nitrogen has been used as carrier gas with a whole gas flow at 75 m^3/h. The rate carrier gas, or rather the part of the gas flow devoted to carry through the powder feeder and drag the powders to the nozzle has been varied in the range of 2.5-3.5 m^3/h according to the data reported in Table 1 and with regard to the different requirements for each mixture. Usually, mixtures containing higher ceramic content exhibit lower flowability and hence require higher carrier gas flow. The gun traverse speed was also tuned to obtain a whole coating thickness in the range of 150-200 µm for all mixtures with a single gun pass. The starting point to optimize the process set up is the deposition protocol employed to deposit pure Ni coating, as Ni constitute the cermet matrix. In particular, regarding the temperature, 500 °C has been selected as main gas temperature to balance the different effects observed as a function of the spray of different blends: from one side in the case of high alumina content in the blend (75 and 90 wt.%), the high gas temperature is critical leading to quite severe wear of the internal walls of the nozzle, due to the scratch of shaped alumina particles. A related loss of performance could be observed, in particular because of the metal particle adhesion at the nozzle walls and the related occurrence of clogging events during spray. From the other side, in the case of very low alumina content (0-10-25 wt.%), the high gas temperature is also critical leading

Table 1 Coldspray deposition parameters

Nozzle	Type 24 (custom pre-heated chamber)							
Alumina type	Shaped, −27 + 17 μm						Spherical agglomerated	
wt.% of Al_2O_3 in the feedstock	0	10	25	50	75	90	10	50
Gas pressure, bar	26.0	26.5	26.3	27.0	27.0	26.5	27.0	27.0
Gas quantity, m^3/h	75.0						75.0	
Process temperature, °C	500						500	
Rate carrier gas, m^3/h	2.1	2.5	3.1	3.2	3.5	3.5	2.1	
Traverse speed, mm/s	200	150	110	90	70	10	50	30
Pass height, mm	1						1	
Standoff distance, mm	20						20	

to the metal particle oxidation during spray. Granted that the oxidation of metal particles occurs in the same way in all blends; it must be considered that in the low blended feedstock there is a minor effect of hard ceramic particle impingement in growing coating and as a consequence lower plastic deformation, lower erosion, and lower rupture of thermally oxidized surface shells of metal particles. In this sense, 500 °C is high enough to allow plastic deformation and to obtain compact microstructure, sufficient adhesion, and cohesion for the required application; it is low enough to avoid thermal oxidation of both substrate and growing coating.

2.4 Characterization

Metallographic samples were prepared by cutting the deposited coatings along the longitudinal cross section, parallel to the spraying direction; subsequently, they were grinded using SiC grit paper, and finally polished up to 1 μm surface finish. The microstructures of these samples were observed in a LEICA DMR optical microscope, and it was also analyzed by electron microscopy. A Hitachi S-3400 scanning electron microscope (SEM), equipped with energy dispersive x-ray microanalysis, was used. Secondary and backscattered electron images (BEI) were obtained. Image analysis was used to determine alumina content and porosity, by computer analysis equipped with *SPIP v4.6.0* software.

Microhardness tests were made in a Buehler Micromet 2101. A Vickers tip, with 500 gf of test load, was employed for these tests. Measurements were done conforming to the norm, *DIN 50133*. Each sample was tested considering 20 measurements, and the final result is the average of all valid measurements.

X-ray diffraction (XRD) analyses were performed using a Philips PW3040/00 X'Pert MPD/MRD diffractometer using Cu-K_α. Patterns were obtained from the top surface of the as-sprayed coatings to characterize the main phases present at the coating surface.

2.5 Oxidation at High Temperature

Several samples with 75 wt.% Al_2O_3 content in the feedstock powders were oxidized in air at 520 °C for 24, 48, 72, 168, and 336 h, in a furnace (Thermconcept Lac Km 20/08/A). The oxidized samples were analyzed by SEM and XRD as it has been described previously.

3. Results and Discussion

3.1 Microstructure

As-deposited coatings obtained by means of the different mixtures with different alumina contents were characterized by light optical microscopy to observe their microstructure, substrate-coating interface, and ceramic particles distribution. Figure 3 shows the cross-sectional views for all sprayed conditions, including the Ni pure coating.

All coatings are constituted of ceramic alumina particles embedded in a pure Ni matrix, as could be observed in Fig. 3 micrographs from pure Ni (Fig. 3a) to the maximum ceramic content investigated, 90 wt.% in the initial feedstock (Fig. 3e). There is a quite homogeneous distribution of ceramic particles in the matrix, and no macroscopic evidences of oxidation in the metal part of the coatings (qualitatively evaluated by microscopic observation and SEM-EDS analysis) were found. Concerning the CS deposition, a ductile metal and a brittle ceramic behave oppositely in CS deposition, and the growth of a composite cermet coating combines different mechanisms. The first concept is that only metal particles are plastically deformed during impact and so they can positively concur to the coating growth. As widely reported in literature, pure ceramic coatings cannot be deposited by CS (Ref 25), and for this reason, ceramic particles could be roughly considered as a passive filler, occasionally entrapped by incoming metal particles and then embedded in the cermet during the coating growth. However, ceramic particles have some important roles in modifying the coating growth and, as a consequence, the coating properties. In this sense, three important effects could be emphasized during spray of metal-ceramic blend. Figure 4 shows schematically the observed mechanisms of both metal and ceramic particles impacting on a growing cermet coating exhibiting on its surface, metal and ceramic composition. Figure 4(a) and (b) shows the mechanisms responsible of the coating growth: First, the growth arising from the impact of a metal particle on a metal substrate thanks to the plastic deformation, depending on particle velocity and temperature, as it has been widely reported in literature (Ref 32). Second, the effect of embedding ceramic particles when they impact on a metal substrate. The plastic deformation of the substrate and the consequent ceramic entrapment. Third,

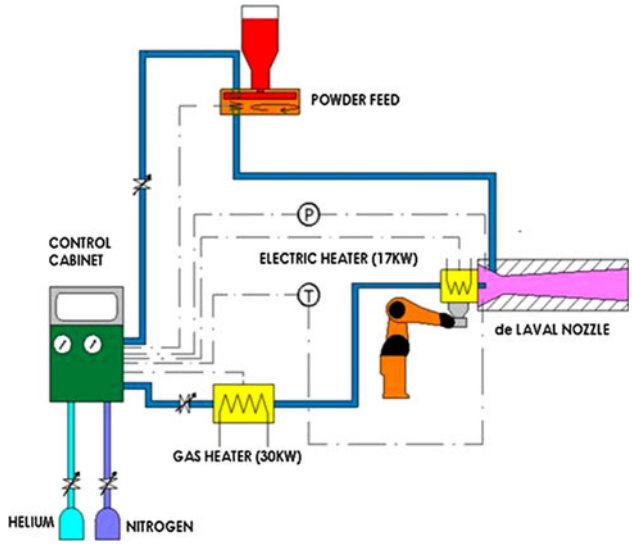

Fig. 2 Schematic diagram of CS process

as shown in Fig. 4(c), the peening effect produced by the impact of a ceramic particle on a metal particle in the growing coating and rebounded by the substrate: this acts as a traditional shot peening process inducing a more severe plastic deformation in the metal particle, an increase of the compressive residual stress, and in some cases, a grain refining. This effect is a function of ceramic/metal-impinging rate, and it is independent on the successive embedding or rebound of the ceramic particle. Owing to the impact geometry, it is intuitive that shaped ceramic particles are more effective in this effect with respect to spherical or agglomerated particles. Very similar considerations could be stated also in the case of Fig. 4(d) when the incoming metal particles impact to embedded ceramic in the growing coating. In that case, the increase in plastic deformation of the incoming metal particle is due to the higher stiffness and hardness of the ceramic that in this moment is acting as a local substrate. Both these effects could be related to the number of ceramic/metal and metal/ceramic impacts which happens in the coating growth, or more simply to the ceramic content in the blend and in the coating. The higher is the ceramic content in the blend (and as a consequence in the coating), the higher is the ceramic/metal particles ratio in the spraying flow and the higher is the number of both impacts: ceramic particles to the growing metal particles, Fig. 4(c); and metal particles to the embedded ceramic particles, Fig. 4(d). Hence, it is expected that the increase in ceramic content in the blend leads to an increase in ceramic content in the coating as well as the increase in compressive residual stress, coating hardness, and brittleness. There is a third effect operating for ceramic content higher than 50 wt.% in the case of cermets mixture investigated in this study—it is the fragmentation of ceramic particles due to the impact of one or more incoming ceramic particles onto an embedded ceramic particle as shown schematically in Fig. 4(e). This is due to the brittleness of aluminum oxide combined with the high velocity of impact. The fragmentation happens when an incoming ceramic particle impact on a deposited ceramic particle. The already deposited ceramic particle is fractured by the impact and the particle debris is finely embedded and spread in the matrix while the incoming ceramic particle is inefficient in the deposition and is rebounded.

Micrographies (e) and (f) in Fig. 3 show the reduction of the mean particle size of aluminum oxide as well as the continuous change in morphology moving from isolated embedded particles in a 3D homogeneous array as reported in (a) through (e) to more aligned particles' distribution as in a pseudo-lamellar morphology as reported in (f). This morphology appears similar to the splats obtained by thermal spray, but there is no melting of the particles or splats in the growing mechanism in CS, and so the morphology is only arising from the geometrical alignment of particles during spray and from the particles rearrangement after the impacts and fragmentations events. Each alumina particle is always surrounded by metal, and no agglomeration of ceramic particles is observed.

A final remark concerns the variation of coating thickness as a function of the increase of the alumina content in the powder mixture due to the different blend-flowing abilities and deposition efficiencies between metal and ceramic powders. As reported in literature (Ref 31, 33, 34), some wt.% of ceramic powders in the feedstock slightly increase the deposition efficiency while higher content lead to a progressively reduction in the whole deposition efficiency. For these reasons, small variations in cold-spray setup parameters, and in particular, an adjustment in the powder feed rate through a combined variation in rate carrier gas and feeder rotation, as reported in Table 1, are operated to adjust the coating growth kinetic and to obtain a final coating thickness of around 100-200 μm. The overall coating porosity is very low, as can be seen in the cross-sectional micrographs reported in Fig. 5. CS technique generally produces coatings characterized by a very low porosity, owing to the high plastic deformation and cold work that is exerted on the particles of metal phase. The continuous high-velocity impingement of particle has the effect to fill the voids and micropores which would be among the deposited particles. Hard, shaped ceramic particles contribute to this effect. Although they do not deform plastically induce further deformation on metal particles, decreasing the overall porosity. The quantitative evaluation of porosity is difficult for cermet coatings by using image analysis procedure, because of the presence of both pores and ceramic fillers, and in particular for coatings exhibiting high ceramic content. However, the porosity could be evaluated in the case of pure Ni and cermet with low ceramic content, and it is rated less than 3%. In this sense, ceramic fragmentation seems to have negligible effect on the overall porosity even if different porosity evaluation techniques must be employed to have quantitative results.

3.2 Alumina Content

The ceramic content increment is not linear with the feedstock content (Fig. 6), owing to the different deposition

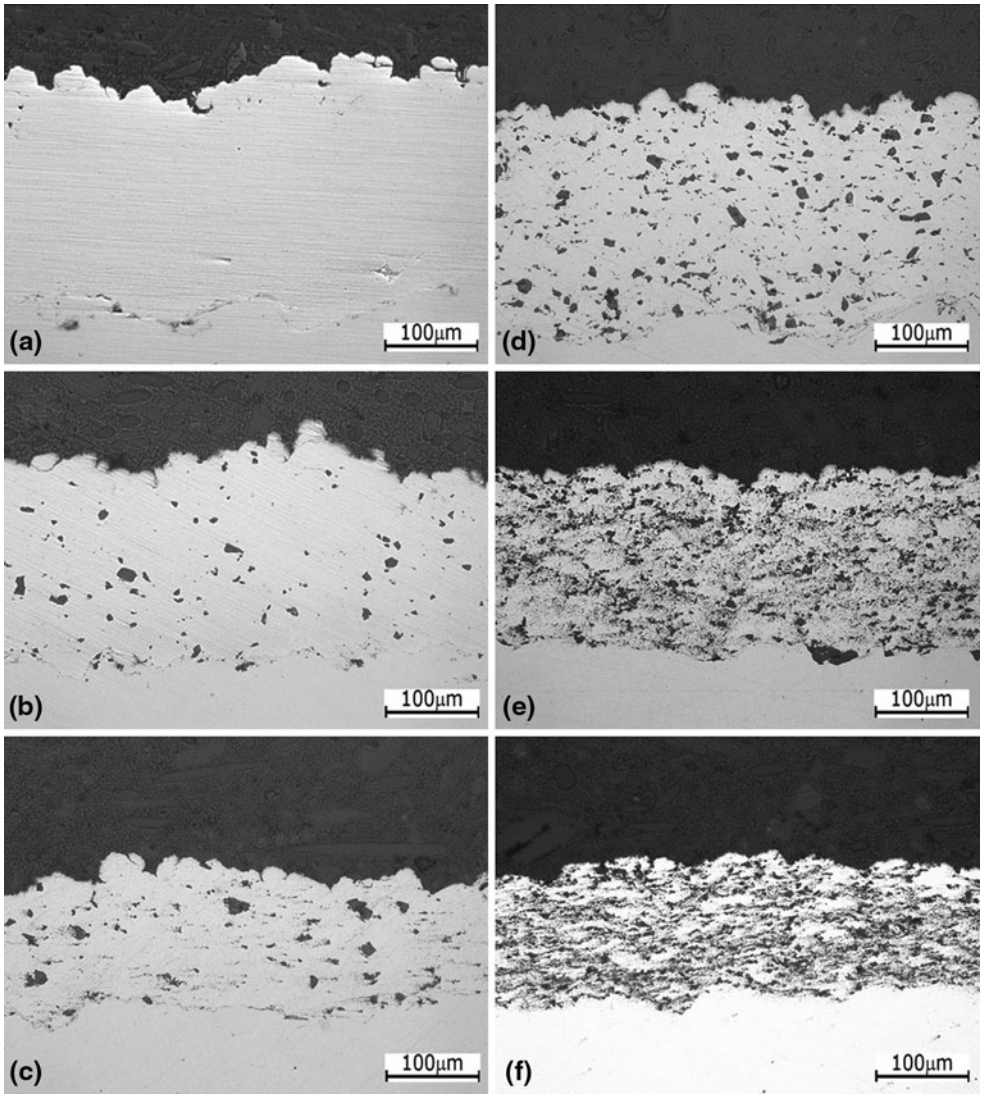

Fig. 3 Cross-sectional views of the coatings with different contents of Al_2O_3 in the feedstock powders: (a) pure Ni; (b) 10% Al_2O_3; (c) 25% Al_2O_3; (d) 50% Al_2O_3; (e) 75% Al_2O_3; and (f) 90% Al_2O_3

efficiency of both materials constituting the mixture. As discussed previously, Ni particles are ductile and promote the coating formation by deforming plastically and bonding to the substrate interface. On the other side, ceramic particles are unable to provide plastic deformation and could only be embedded into Ni metal phase.

The behavior of Al_2O_3 content embedded in the coatings as a function of Al_2O_3 content in the initial feedstock is reported in Fig. 6. The ceramic content has been evaluated by image analysis data obtained using software SPIP v4.6.0. Surface covering was evaluated and converted first to volume and then to weight percentage. The dashed line shows the ideal ceramic content in the coating if the initial composition of the feedstock would be respected. A dual trend could be emphasized with a critical point of around 50 wt.% ceramic content in the initial feedstock. The effectiveness of embedding ceramic, embedding efficiency defined as the ratio between the percentage of ceramic particle contained in the feedstock and the percentage of ceramic particle in the deposited coating, is very low for feedstock with lower ceramic content reaching a maximum value of about 8 wt.% at 50 wt.% initial feedstock (16% of embedding efficiency); while for ceramic-richer feedstock, the effectiveness of embedding increase reaches ceramic contents of 16 and 31 wt.% (21 and 34% embedding efficiencies, respectively). An hypothesis for this increase is the fragmentation of ceramic particles during impact which could promote the effectiveness of the embedding mechanism; however, further experimental evidences are required to confirm this hypothesis.

3.3 Use of Spherical Alumina

The alumina fragmentation during CS is a key feature for the design and realization of micro and nanostructured cermets coatings starting from powder blends of

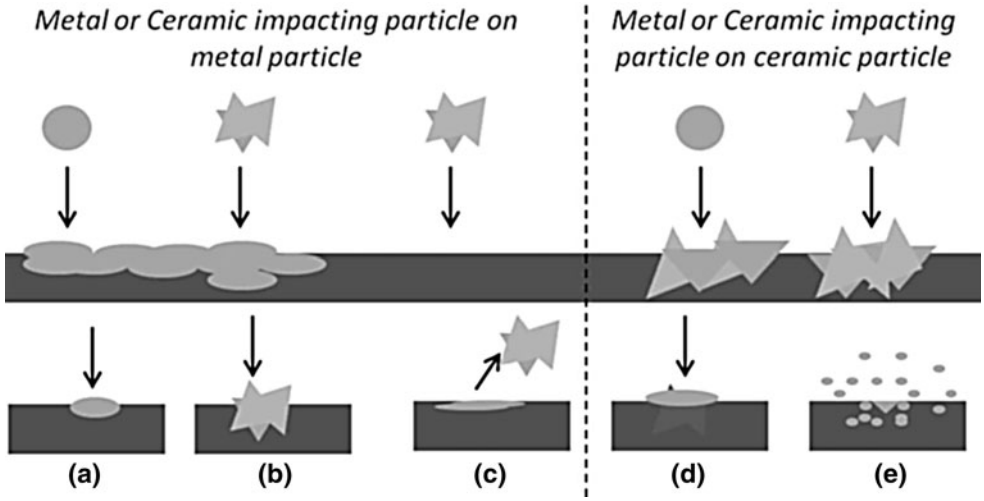

Fig. 4 Schematic representation of different impacting effects during the deposition of cermet coating by coldspray starting from a powder blend. (a) Coating growth by impact of metal particle on metal substrate. (b) Coating growth by embedding of ceramic particle on metal substrate. (c) Cold work induced by peening of ceramic particles on deposited metal particles. (d) Cold work (and coating growth) induced by deposition of metal particles on embedded ceramic particles. (e) Ceramic particle fragmentation due to high velocity impact of ceramic particle on an embedded ceramic particle

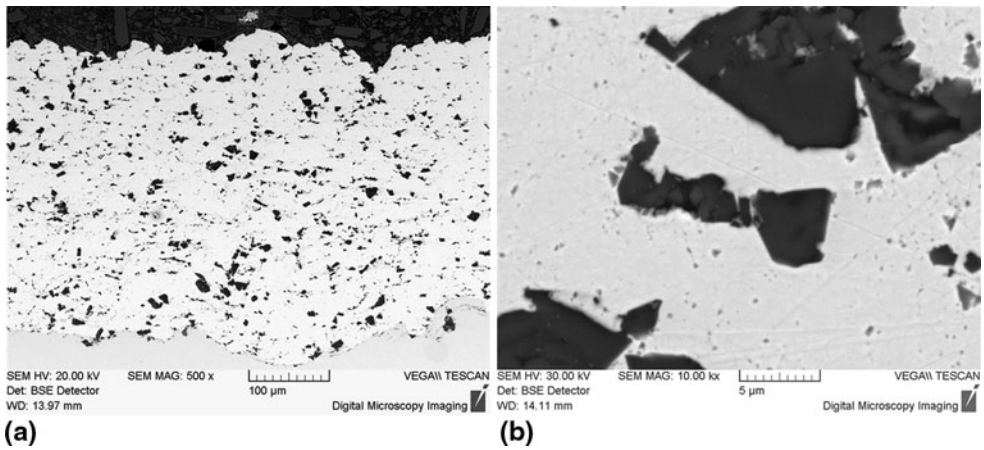

Fig. 5 BEI corresponding to Ni-50% Al_2O_3 cermets showing overall porosity. (a) Panoramic view. (b) Higher magnification image

traditional commercial powders. Ni-Al_2O_3 deposited coatings exhibit a reduction of ceramic particles mean size, up to few micron, with noticeable sub-micrometric fraction and they also exhibit a more homogeneous ceramic particles distribution in the coating matrix. Furthermore, it is well known that a finer distribution of smaller particles is more desirable with respect to few big particles in the design of a cermet. For example, smaller ceramic particles avoid erosion and third body abrasion in friction applications, they reduce the stress amount at the edge of shaped ceramic particles and reduce crack generation and propagation under different mechanical loads; they support the grain refining in metal matrix and act as a barrier in crack propagation. It is also expected that they could be more effective in increasing solar absorption and reducing the emission performances. (Ref 35)

However, ceramic particles fragmentation occurs only using ceramic-rich blends with alumina up to 50 wt.% representing a limitation in the coating design and avoiding the possibility to have finer ceramic particles at percentage lower than 20 wt.%. For this reason, the use of spherical agglomerated aluminum oxide particles, shown in Fig. 7, has also been tested to achieve finer ceramic particle mean size and more homogeneous dispersion in the metal matrix. In fact, agglomerated particles are composed of nano-constituents weakly bonded between each other, and as a consequence, a larger fragmentation effect is expected during spray leading to a finer dispersion of ceramic into the coatings. However, owing to the high particle velocity, the fragmentation events are too violent with the occurrence of ceramic particle explosion at the instant of the impact to the substrate. A nanoparticles cloud forms near the spray zone because of the particle explosion and rebound. Two different mixes have been tested containing, respectively 10 and 50 wt.% of alumina in blend with Ni. The CS parameters are reported in

Table 1 and in particular the gas temperature and the carrier gas flow have been set to 500 °C and 75 m^3/h, respectively, according to the conditions employed for spraying the blends with shaped alumina. The micrographies of cross-sectioned CS coatings are shown in Fig. 7(c) and (d), respectively in the case of 10 and 50 wt.% alumina blends. The growth behavior is noticeable different by changing the alumina content in the feedstock: in the case of 10 wt.% alumina, a slight increase in porosity is observed even if the coating microstructure is very close to the coating microstructure obtained by using shaped alumina. The embedded alumina is preferentially un-fragmented, micrometric sized and quite homogeneously dispersed in the Ni matrix. On the other side, no noticeable growth is reported in the case of spraying the 50 wt.% alumina feedstock and the maximum coating thickness is typically lower than 100 μm; the alumina spread along the coating surface hindering the plastic deformation of metal particles and hence the coating growth. The criticity seems to be the weakness of the bond between the nanoparticles constituting the agglomerates and the related particle fragmentation and explosion. While particle fragmentation of shaped ceramic alumina occurs on the already embedded ceramic particles leading to a mean size reduction of the embedded ceramic as previously discussed, the fragmentation of spherical agglomerated particles occurs at the instant of impact leading to the formation of a nanoparticle cloud with no efficient embedding.

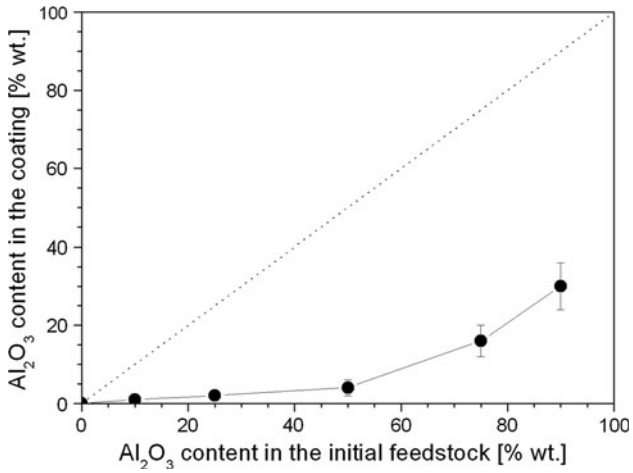

Fig. 6 Aluminum oxide content in the coating with respect to content in the initial powder blend

3.4 Microhardness

Microhardness tests were performed into Ni matrix to evaluate the influence of Al_2O_3 particles on the metal hardness. The results are presented in Fig. 8 which shows an increment of hardness as the ceramic content is increased. 175 ± 5 HV0.5 was measured for the pure Ni CS coating while 338 ± 17 HV0.5 was the hardness for the coating with 90% Al_2O_3 in the feedstock powder. The hardness measured for the CS pure Ni is higher than the typical values of bulk materials (around 70-80 HV) because of the high deformation induced during CS, which is responsible of a noticeable work hardening of the

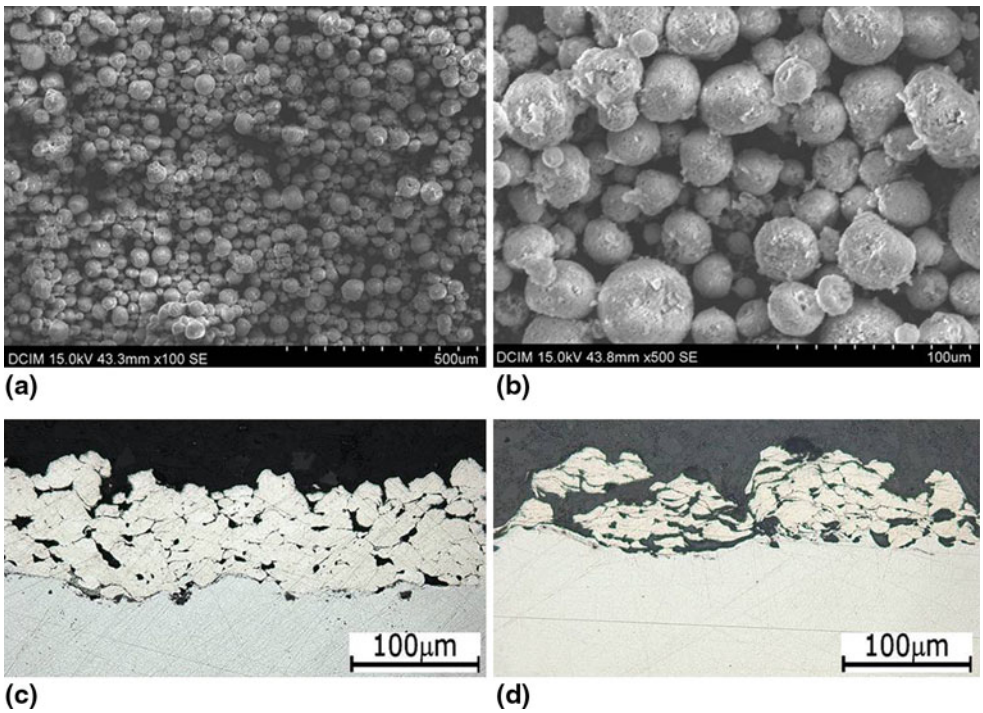

Fig. 7 (a, b) SEM views of the considered feedstock powders. Cross-sectional micrography of a cold-sprayed coating obtained starting from: (c) 10:90 wt.% alumina:nickel blend. (d) 50:50 wt.% alumina:nickel blend

metallic phase. The ceramic particles increased the hardness of the coating by several reasons. On one hand, higher hardness has been traditionally observed in metal matrix composites, compared with the unreinforced counterparts, because of microstructural changes induced by the reinforcements (Ref 36-38). On the other hand, it could be expected that a higher number of ceramic particles will induce more work hardening on the metal phase because of an increment on the number of collisions as it has been discussed previously.

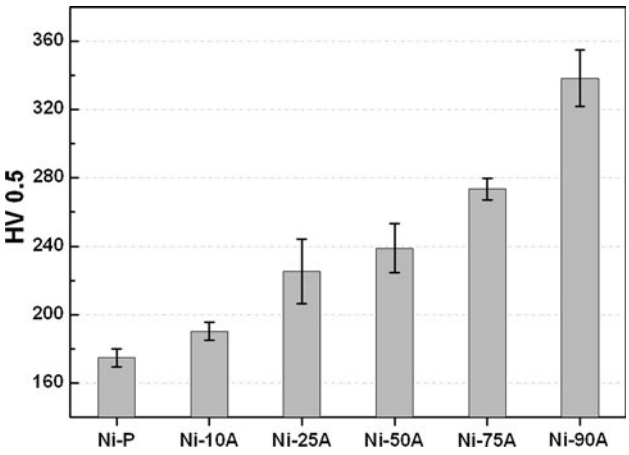

Fig. 8 Evolution of microhardness vs. ceramic content

3.5 Oxidation at 520 °C

During oxidation at 520 °C, a thin oxide layer was formed at the coating surface, even for the shortest exposure time, as it could be observed in Fig. 9. The morphology of this layer was not modified with the exposure time, but the thickness increased from around 1 μm after 24-h (Fig. 9(a) exposure up to around 4 μm after 336-h exposure at 520 °C (Fig. 9c, d). The oxides formed during oxidation were located at the coating surface, even for the longest exposure times (Fig. 9d), and no oxidation was observed through the coating thickness close to the substrate. Only some oxides penetrated through the porosity associated to the ceramic particles located close to the top surface of the cermet (Fig. 9c). However, oxidation did not penetrate through the coating because there is no interconnected porosity and, consequently, the penetration of the aggressive species is more complicated in these coatings. This behavior constitutes a clear advantage in comparison with other high-temperature thermal-spraying techniques, which usually exhibit interconnected porosity with detrimental effects for high-temperature performance.

XRD analysis identified the oxides formed during exposition at 520 °C as NiO. Figure 10 shows XRD traces

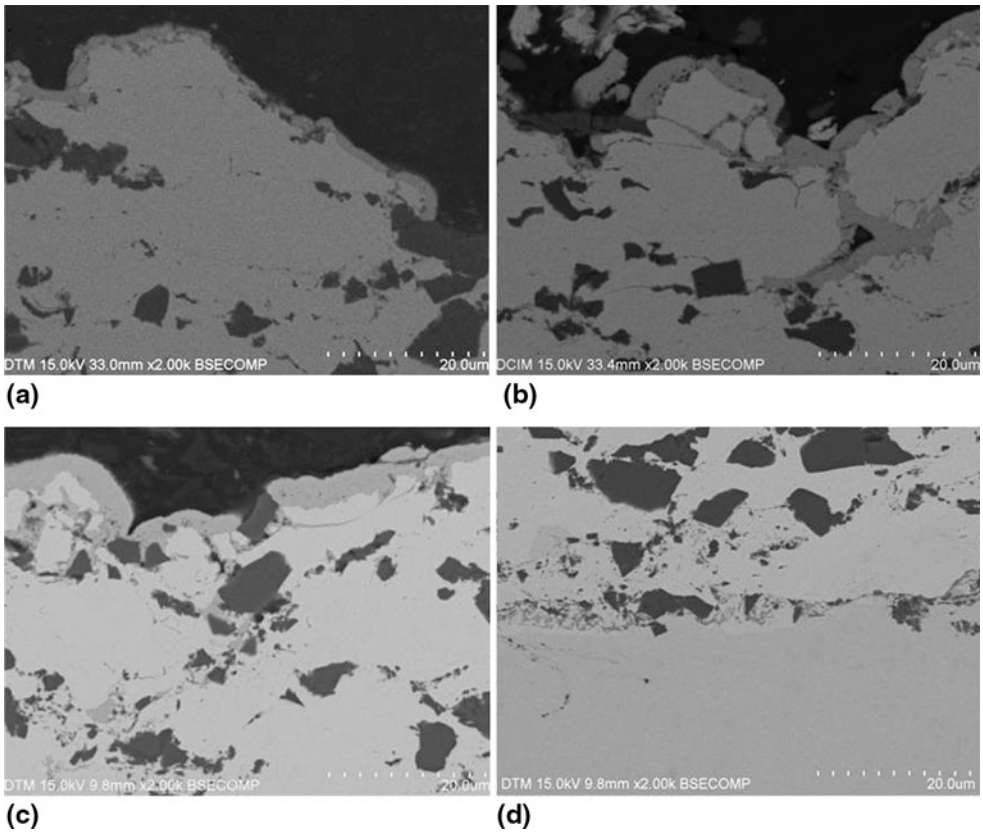

Fig. 9 BEI corresponding to the Ni-75% Al_2O_3 coatings after oxidation in air at 520 °C for exposures of 24 (a), 168 (b), and 336 (c and d) h

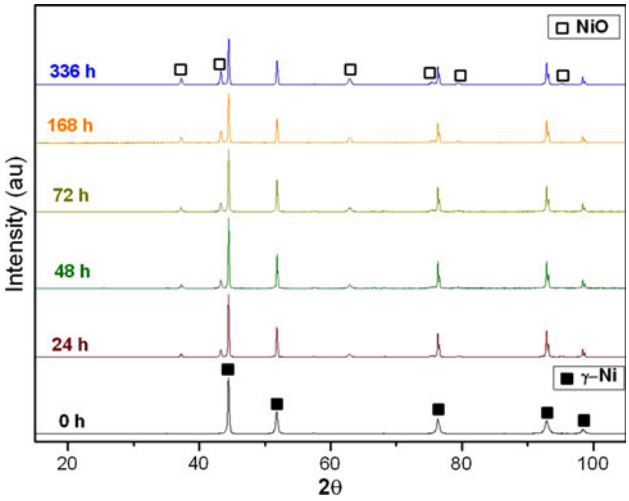

Fig. 10 XRD traces of the Ni-75% Al_2O_3 coatings after oxidation in air at 520 °C for 24, 48, 72, 168, and 336 h. The pattern corresponding to the as-sprayed coating is also included for comparison purposes

corresponding to the oxidized samples as well as to the as-sprayed coating. As should be expected, γ-Ni (*Fm3m* space group, $a = 0.352$ nm) was the dominant phase before oxidation. After exposure at high-temperature, peaks corresponding to NiO (*Fm3m* space group, $a = 0.417$ nm) were detected. The intensity of these peaks was increased with the increasing exposure time, indicating an increment of oxide content in agreement with the images observed by SEM.

4. Conclusions

According to the experimental results obtained in this study, the following conclusions can be drawn:

(a) Composite Ni-Al_2O_3 cermet coatings could be deposited in a wide range of composition by CS technology which microstructure consisting of Al_2O_3 particles bound together by a Ni matrix.

(b) Increasing ceramic content in feedstock powder leads to a higher ceramic content in final coating, but without agglomerate forming; however, a homogeneous particle distribution is observed even for the highest ceramic content conditions.

(c) Ceramic particle fragmentation and mean size reduction in coating microstructure are observed for spraying blend with ceramic content higher than 50 wt.%.

(d) Porosity is negligible for these cold-sprayed coatings, being lower than 3%. This porosity is mainly located at broken ceramic particles, forming voids caused for the high stresses because of the impingement of subsequent particles. However, no interconnected porosity was detected.

(e) The use of spherical agglomerated alumina particles has been explored and compared with the shaped one. A slight increase in coating porosity and a reduction in deposition efficiency are reported when using 10 wt.% blend, while negligible coating growth is reported when using 50 wt.% alumina feedstock.

(f) CS of pure Ni exhibited a hardness higher than that typically observed in bulk materials, due to the work hardening induced during CS. The ceramic particles increased the hardness of the coating from 175 ± 5 HV0.5 for the pure Ni up to 338 ± 17 HV0.5 for the coating with 90% Al_2O_3 in the feedstock. The number of collisions is increased, as the number of particles is higher, promoting a greater work hardening.

(g) Preliminary oxidation tests show these coatings as possible candidates for high-temperature applications. The performance at high temperature is enhanced by the absence of interconnected porosity.

Acknowledgments

The authors would like to thank the Spanish government CICYT through grant MAT2010-18916 and *Universidad Rey Juan Carlos* through the projects CCG10-URJC/MAT-5550 and "Comportamiento de recubrimientos con aplicaciones a alta temperatura" for financial support. A special thanks to Francisco Sevillano for his job and collaboration.

References

1. R. Rajendran, Gas Turbine Coatings—An Overview, *Eng. Fail. Anal.*, 2012, **26**, p 355-369
2. C.W. Lee, J.H. Han, J. Yoon, M.C. Shin, and S.I. Kwun, A Study on Powder Mixing for High Fracture Toughness and Wear Resistance of WC-Co-Cr Coatings Sprayed by HVOF, *Surf. Coat. Technol.*, 2010, **204**(14), p 2223-2229
3. A.K. Basak, J.-P. Celis, P. Ponthiaux, F. Wenger, M. Vardavoulias, and P. Matteazzi, Effect of Nanostructuring and Al Alloying on Corrosion Behaviour of Thermal Sprayed WCCo Coatings, *Mater. Sci. Eng. A*, 2012, **558**(15), p 377-385
4. C. Feng, V. Guipont, M. Jeandin, O. Amsellem, F. Pauchet, R. Saenger, S. Bucher, and C. Iacob, B4C/Ni Composite Coatings Prepared by Cold Spray of Blended or CVD Coated Powders, *Proc. ITSC 2011*, 27-29 Sep 2011, Hamburg
5. D. Sporer, M. Dorfman, L. Xie, A. Refke, I. Giovannetti, and M. Giannozzi, Processing and Properties of Advanced Ceramic Abradable Coatings, *Thermal Spray 2007: Global Coating Solutions*, B.R. Marple, M.M. Hyland, Y.-C. Lau, C.-J. Li, R.S. Lima, and G. Montavon, Eds., ASM International, Materials Park, OH, 2007, p 495-500
6. D. Sporer, A. Refke, M. Dratwinski, M. Dorfman, I. Giovannetti, M. Giannozzi, and M. Bigi, Increased Efficiency of Gas Turbines, *Sulzer Tech. Rev.*, 2008, **2**, p 4-7
7. Sulzer-Metco, "Improve Efficiency and Reduce Emissions with High Pressure Turbine Abradable Coatings for Industrial Gas Turbines", Solutions Flash, Sulzer-Metco SF-0015.0a, 2009, 8 p
8. United Nations "Kyoto Protocol" December 11th 1997, Kyoto
9. S.A. Kalogirou, Solar Thermal Collectors and Applications, *Prog. Energy Combust. Sci.*, 2004, **30**, p 231-295
10. C.E. Kennedy, "Review of Mild-to-High-Temperature Solar Selective Absorbers Materials", Technical Report National Renewable Energy Laboratory, NREL/TP-520-31267, 2002

11. A. Hall, A. Ambrosini, and C. Ho, Solar Selective Coatings for Concentrating Solar Power Central Receiver, *Adv. Mater. Process.*, 2012, **170**(1), p 28-32
12. S. Wijewardane and D.Y. Goswami, A Review on Surface Control of Thermal Radiation by Paints and Coatings for New Energy Applications, *Renew. Sustain. Energy Rev.*, 2012, **16**, p 1863-1873
13. V. Teixeira, E. Sousa, M.F. Costa, C. Nunes, L. Rosa, M.J. Carvalho, M. Collares-Pereira, E. Roman, and J. Gago, Spectrally Selective Composite Coatings of Cr-Cr_2O_3 And Mo-Al_2O_3 for Solar Energy Applications, *Thin Solid Films*, 2001, **392**, p 320-326
14. C. Nunes, V. Teixeira, M. Collares-Pereira, A. Monteiro, E. Roman, and J. Martin-Gago, Deposition of PVD Solar Absorber Coatings for High-Efficiency Thermal Collectors, *Vacuum*, 2002, **67**, p 623-627
15. D. Xinkang, W. Cong, W. Tianmin, Z. Long, C. Buliang, and R. Ning, Microstructure and Spectral Selectivity of Mo-Al_2O_3 Solar Selective Absorbing Coatings After Annealing, *Thin Solid Films*, 2008, **516**, p 3971-3977
16. S. Esposito, A. Antonaia, M.L. Addonizio, and S. Aprea, Fabrication and Optimisation of Highly Efficient Cermet-Based Spectrally Selective Coatings for High Operating Temperature, *Thin Solid Films*, 2009, **517**, p 6000-6006
17. V.K. Champagne, *The Cold Spray Materials Deposition Process: Fundamentals and Applications*, Woodhead Publishing in Materials, Philadelphia, ISBN-13: 978-1420066708
18. Li C-X, Li C-J, and L.-J. Guo, Performance of a Ni/Al_2O_3 Cermet-Supported Tubular Solid Oxide Fuel Cell Operating With Biomass-Based Syngas Through Supercritical Water, *Int. J. Hydrogen Energy*, 2010, **35**, p 2904-2908
19. Li C-X, L.-L. Yun, Y. Zhang, and C.-J,L.-J. Guo, Microstructure, Performance Cermet Supported SOFC Operating Using Supercritical Water, *Int. J. Hydrogen Energy*, 2012, **37**, p 3001-3006
20. Sulzer-Metco, ''Thermal Spray Coating Solutions for Solid Oxide Fuel Cells Perovskite Coatings—Dense, Thin Electrolytes—Insulating Layers'', Solutions Flash, Sulzer-Metco SF-0012.1a, 2009, 8 p
21. G. Bolelli, V. Cannillo, L. Lusvarghi, and T. Manfredini, Wear Behaviour of Thermally Sprayed Ceramic Oxide Coatings, *Wear*, 2006, **261**, p 1298-1315
22. V. Fervel, B. Normand, and C. Coddet, Tribological Behavior of Plasma Sprayed Al_2O_3-Based Cermet Coatings, *Wear*, 1999, **230**, p 70-77
23. X.C. Zhang, B.S. Xu, S.T. Tu, F.Z. Xuan, H.D. Wang, and Y.X. Wua, Fatigue Resistance and Failure Mechanisms of Plasma-Sprayed CrC-NiCr Cermet Coatings in Rolling Contact, *Int. J. Fatigue*, 2009, **31**, p 906-915
24. S. Rech, A. Trentin, S. Vezzù, J.-G. Legoux, E. Irissou, and M. Guagliano, Influence of Pre-Heated Al 6061 Substrate Temperature on the Residual Stresses of Multipass Al Coatings Deposited by Cold Spray, *J. Therm. Spray Technol.*, 2011, **20**(1-2), p 243-251
25. A. Payrin, V. Kosarev, S. Klinkov, A. Alkimov, and V. Fomin, *Cold Spray Technology*, Elsevier, Amsterdam, 2007
26. T. Schmidt, H. Assadi, F. Gärtner, H. Richter, T. Stoltenhoff, H. Kreye, and T. Klassen, From Particle Acceleration to Impact and Bonding in Cold Spraying, *J. Therm. Spray Technol.*, 2009, **18** (5-6), p 794-808
27. J. Vlcek, L. Gimeno, H. Huber, and E. Lugscheider, A Systematic Approach to Material Eligibility for the Cold-Spray Process, *J. Therm. Spray Technol.*, 2005, **14**(1), p 125-133
28. W.-Y. Li, C. Zhang, H. Liao, J. Li, and C. Coddet, Characterization of Cold-Sprayed Nickel-Alumina Composite Coating with Relatively Large Nickel-Coated Alumina Powder, *Surf. Coat. Technol.*, 2008, **202**, p 4855-4860
29. H. Koivuluoto and P. Vuoristo, Effect of Ceramic Particles on Properties of Cold-Sprayed Ni-20Cr + Al_2O_3 Coatings, *J. Therm. Spray Technol.*, 2009, **18**(4), p 555-562
30. J.O.- Kielmann, H. Gutzmann, F. Gärtner, H. Hübner, C. Borchers, and T. Klassen, Formation of Cold-Sprayed Ceramic Titanium Dioxide Layers on Metal Surfaces, *J. Therm. Spray Technol.*, 2011, **20**(1-2), p 292
31. E. Irissou, J.-G. Legoux, B. Arsenault, and C. Moreau, Investigation of Al-Al_2O_3 Cold Spray Coating Formation and Properties, *J. Therm. Spray Technol.*, 2007, **16**(5-6), p 661
32. H. Assadi, F. Gartner, T. Stoltenhoff, and H. Kreye, Bonding Mechanism in Cold Gas Spraying, *Acta Mater.*, 2003, **51**, p 4379-4394
33. A. Sova, A. Papyrin, and I. Smurov, Influence of Ceramic Powder Size on Process of Cermet Coating Formation by Cold Spray, *J. Therm. Spray Technol.*, 2009, **18**(4), p 633
34. A. Shkodkin, A. Kashrin, O. Klyuev, and T. Buzdygar, Metal Particle Deposition Stimulation by Surface Abrasive Treatment in Gas Dynamic Spray, *J. Therm. Spray Technol.*, 2006, **15**(3), p 382
35. V. Viswanathan, T. Laha, K. Balani, A. Agarwal, and S. Seal, Challenges and Advances in Nanocomposite Processing Techniques, *Mater. Sci. Eng. R*, 2006, **54**, p 121-285
36. D.J. Lloyd, Particulate Reinforced Aluminum and Magnesium Matrix Composites, *Int. Mater. Rev.*, 1994, **39**, p 1-23
37. T.W. Clyne and P.J. Withers, *An Introduction to Metal Matrix Composites*, Cambridge University Press, Cambridge, 1993
38. J. Rodríguez, M.A. Garrido-Maneiro, P. Poza, and M.T. Gómez-del Río, Determination of Mechanical Properties of Aluminium Matrix Composites Constituents, *Mater. Sci. Eng. A*, 2006, **437**, p 406-412